JOURNAL OF SPACECRAFT AND ROCKETS
Vol. 31, No. 6, November–December 1994

Supersonic Near-Wake Afterbody Boattailing Effects on Axisymmetric Bodies

J. L. Herrin* and J. C. Dutton†
University of Illinois at Urbana–Champaign, Urbana, Illinois 61801

An experimental investigation of the near-wake flowfield downstream of a conical boattailed afterbody in supersonic flow is presented. The afterbody investigated is typical of those for conventional boattailed missiles and projectiles in unpowered flight. Flow visualization, mean static pressure measurements, and three-component laser Doppler velocimeter data have been obtained throughout the near wake of the body. The effects of afterbody boattailing on the physics of the near-wake flow are determined by comparing the present data with similar data obtained on a cylindrical afterbody. Results indicate that a net afterbody drag reduction of 21% is achieved with the current boattailed afterbody for a freestream Mach number of 2.46. The shear-layer growth rate, and therefore mass entrainment from the recirculation region behind the base, is shown to be significantly reduced by afterbody boattailing due to the reduction in turbulence levels throughout the near wake as compared to the cylindrical afterbody.

Nomenclature

C_D = dimensionless drag coefficient
C_f = skin-friction coefficient
C_p = dimensionless pressure coefficient
d = hole diameter, mm
H = compressible shape factor, δ^*/θ
k = turbulent kinetic energy, m^2/s^2
M = Mach number
R_0 = afterbody radius upstream of boattail, mm
r = radial coordinate, mm
S = distance to shear-layer reattachment, mm
U = mean axial velocity, m/s
u_τ = friction velocity, m/s
u' = instantaneous axial-velocity fluctuation, m/s
V_r = mean radial velocity, m/s
v = instantaneous velocity, m/s
v_r' = instantaneous radial-velocity fluctuation, m/s
v_t' = instantaneous tangential-velocity fluctuation, m/s
x = axial coordinate, mm
y = distance perpendicular to local afterbody surface, mm
β = afterbody surface angle relative to horizontal, deg
δ = boundary-layer thickness, mm
δ^* = boundary-layer displacement thickness, mm
θ = boundary-layer momentum thickness, mm
ν_w = kinematic viscosity at wall, m^2/s
Π = boundary-layer wake strength parameter
σ = root-mean-square value
$\overline{\langle\ \rangle}$ = ensemble-averaged value
$\overline{(\ )}$ = area-weighted average value

Subscripts

b = boattailed afterbody
base = condition at base
c = cylindrical afterbody
net = sum of boattail and base contributions
u = axial component
v_r = radial component
v_t = tangential component
1 = approach conditions to the afterbody

Received Nov. 3, 1993; presented as Paper 94-0029 at the AIAA 32nd Aerospace Sciences Meeting, Reno, NV, Jan. 10–13, 1994; revision received April 20, 1994; accepted for publication May 26, 1994.

*Graduate Reasearch Assistant; currently employed as a National Research Council Associate, NASA Langley Research Center, M/S 170, Hampton, VA 23681-0001. Member AIAA.

†Professor, Department of Mechanical and Industrial Engineering, 140 Mechanical Engineering Building, 1206 W. Green St. Associate Fellow AIAA.

Introduction

MODERN missiles and projectiles can suffer significant amounts of drag during transonic and supersonic flight due to the low pressure acting on the rear of the body. Generally termed base drag, the pressure-area force acting on the base of a typical flight vehicle can make up a substantial portion of the total drag in many instances, especially for missiles or projectiles in unpowered flight, where a high-pressure propulsive jet is absent.[1] In fact, the base drag on the Space Shuttle Columbia has been shown to be approximately 50% of the total orbiter drag during re-entry.[2] Throughout the last three decades, several methods to reduce base drag have been developed, including afterbody boattailing, base bleed, base cavities, and base burning. The simplest of these to implement in practice is afterbody boattailing, which generally involves only a slight modification to the afterbody surface angle, the payoff being a higher base pressure (reduced afterbody drag). Reference 3 has shown that conical boattails (constant afterbody surface angle β prior to separation) can reduce the net afterbody drag by up to 30% from that on a cylindrical afterbody ($\beta = 0$ deg) in unpowered, supersonic flight. Although the global benefits (i.e., drag reduction) of afterbody boattailing have been well established for different boattail angles, Mach numbers, and Reynolds numbers (e.g., Refs. 4–7), detailed studies of the fluid-dynamic effects in the near wake due to afterbody boattailing have not previously been conducted. An increased understanding of the flow physics in the base region is essential as new methods are developed to further reduce net afterbody drag on practical flight vehicles.

The near-wake flowfield of an axisymmetric, boattailed afterbody in a uniform supersonic flow is sketched in Fig. 1. Several complicated fluid-dynamic phenomena exist in the flowfield, including the rapid expansion of the turbulent boundary layer at the body-boattail junction, geometric boundary-layer separation at the base corner, growth of the compressible shear layer, and reattachment along the axis of symmetry. Obviously, the effects on the near wake of adding a boattail to a cylindrical afterbody stem from the change in initial conditions at the base-corner separation point, which include a higher freestream Mach number, nonzero local flow angle, and nonzero pressure gradient due to the axisymmetric compression effect on the boattail as the flow approaches the axis of symmetry. In addition, the presence of the boattail alters the state of the turbulent

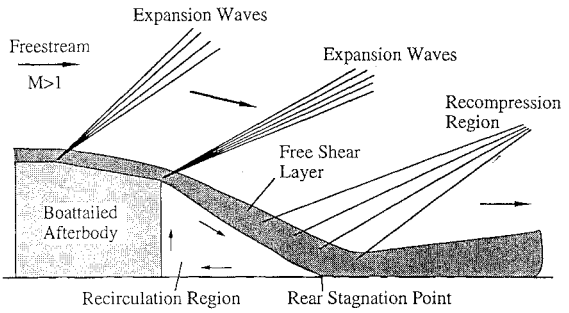

Fig. 1 Schematic diagram of mean flowfield downstream of boattailed afterbody.

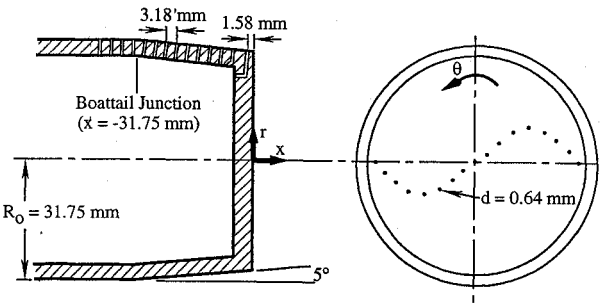

Fig. 2 Diagram of pressure-tap locations and coordinate origin for boattail model.

boundary layer by the rapid expansion at the body-boattail junction and by the adverse pressure gradient on the boattail surface. As will be shown in this paper, the outer inviscid flow over the boattail can be adequately predicted by the axisymmetric method of characteristics; however, the boundary-layer development along the boattail up to the separation point is much more difficult to predict. In addition, the mean and turbulent characteristics of the boundary layer at separation play an important role in determining the initial structure of the separated shear layer and, therefore, the turbulent mixing and mass entrainment rates in the near wake.

Several authors have shown that rapid expansions (such as those at the body-boattail junction and base corner) can significantly distort the mean and turbulence characteristics of an attached turbulent boundary layer. Reference 8 found a significant distortion in the mean-velocity profiles downstream of a variety of centered expansions in supersonic flow. This reference noted the possibility that the distorted postexpansion boundary layer could have a significant effect on the separation characteristics, shear-layer growth rates, and reattachment processes for boattailed afterbodies, the effect being greater for larger boattail angles. It has also been established that rapid expansions reduce the turbulence levels in compressible boundary layers.[9,10] Reference 11 recently used filtered Rayleigh scattering to show that the strong dilatation effect associated with the rapid expansion of a compressible boundary layer increases the scale of the turbulent structures present in the approach boundary layer. In addition, the small-scale turbulence near the wall was shown to recover more quickly from the effects of the expansion than the relatively large-scale motion in the outer region of the boundary layer. The effect of the strong expansion at the body-boattail junction on the afterbody boundary layer and, hence, on the initial conditions to the near-wake flowfield has generally been ignored in previous investigations of boattailed afterbody flowfields.

The primary objective of the present research is to investigate the fluid-dynamic effects of afterbody boattailing on axisymmetric bodies in supersonic flow in an effort to shed new light on the mechanisms associated with the increase in base pressure (reduced afterbody drag) relative to the cylindrical afterbody case. To this end, schlieren and shadowgraph photography, static pressure measurements, and three-component laser Doppler velocimetry (LDV) data have been obtained throughout the near wakes of both a cylindrical afterbody and a boattailed afterbody. The data obtained downstream of the cylindrical afterbody have been presented elsewhere.[12] In this paper measurements with the boattailed afterbody are presented and comparisons with the cylindrical afterbody case are made to determine the fluid-dynamic effects of adding a conical boattail to a cylindrical afterbody. In addition, a complete documentation of the mean velocity and turbulence fields throughout the near wake of a boattailed afterbody will provide a valuable data base to which analytical and numerical modelers of base flows can compare solutions.

Experimental Facility and Instrumentation

The experiments described herein were conducted in the axisymmetric wind-tunnel facility at the University of Illinois Gas Dynamics Laboratory. A detailed description of the axisymmetric wind tunnel and its use for the study of supersonic, axisymmetric afterbody flows has been given in Ref. 12. The mean freestream Mach number is 2.46, the unit Reynolds number is 52×10^6 m^{-1}, and the measured freestream turbulence intensity is less than 1%. Physical support for the afterbody is provided by a cylindrical sting of radius 31.75 mm that extends upstream through the nozzle in order to avoid any flow disturbances in the near wake. The boattail chosen for the present study has a conical shape with an angle relative to the horizontal of 5 deg and an axial length of 31.75 mm (0.5 caliber). Reference 13 has shown that the optimal boattail shape (i.e., shape yielding minimum afterbody drag) is essentially conical at moderate supersonic Mach numbers for typical boattail lengths. In addition, the boattail angle chosen is near the optimal angle given in Ref. 3 for minimum total afterbody drag at Mach 2.5.

Conventional schlieren and shadowgraph photography were used to investigate the overall structure of the near-wake flowfield. These photographs were of only moderate quality because of the axisymmetric nature of the flow, but they were used successfully to confirm the mean flowfield sketched in Fig. 1. Surface oil-streak visualization on the base surface was used to document the symmetry of the near-wake flowfield. By combining motor oil (10W-30) with a black pigment and then applying it to the base in small drops, an oil-streak pattern was observed during a wind-tunnel blowdown and was found to be a very sensitive indicator of flow symmetry at the base.

Mean static pressure measurements were made on the afterbody and base surfaces with a Pressure Systems Inc. digital pressure transmitter (DPT 6400-T). Seventeen taps (0.64 mm in diameter) were located symmetrically across the base at radial intervals of 3.18 mm in order to assess the radial dependence of the time-averaged base pressure. In addition, 14 taps (0.64 mm in diameter) were located on the afterbody surface to document the mean static pressure field approaching and along the boattail. The afterbody taps were separated axially by 3.18 mm in such a way that four taps were located upstream of the body-boattail junction and ten taps were located axially along the boattail. Figure 2 is a schematic diagram showing the pressure-tap locations on the afterbody and base surfaces.

The primary experimental tool used in the current study was a two-component LDV system with frequency shifting, which was used to measure the near-wake velocity field. The optical arrangement and system setup are identical to that used in the cylindrical afterbody case.[12] The measurement-volume diameter and length are approximately 120 and 700 μm, respectively. Data were obtained in two perpendicular planes (horizontal and vertical), each intersecting the axis of symmetry. In the vertical plane, the two-component LDV system measures axial and radial velocities, while in the horizontal plane, the system measures axial and tangential velocities. Hence, two independent planes of LDV data in the near wake were obtained, from which three mean velocities, three Reynolds normal stresses (σ_u^2, $\sigma_{v_r}^2$, and $\sigma_{v_t}^2$), and two of three Reynolds shear stresses ($\langle u'v_r' \rangle$ and $\langle u'v_t' \rangle$) were determined. The LDV measurement grid consisted of approximately 1300 spatial locations concentrated in regions of large velocity gradients (e.g., the separated shear layer). An error analysis of the LDV data acquisition procedure was used to estimate a worst-case uncertainty in the mean velocity of 1.2% of U_1 and in the root-mean-square velocity fluctuation of 2.3% of U_1, where $U_1 = 567$ m/s is the mean freestream velocity approaching the afterbody.

Results

Pressure Measurements

The static pressure distribution along the boattailed afterbody is shown in Fig. 3 along with a method-of-characteristics solution for irrotational, axisymmetric flow. The sharp decrease in pressure through the expansion at the body-boattail junction ($x/R_0 = -1.0$) is clearly evident. The experimental data are shown to relax gradually to the predicted pressure field downstream of the expansion so that near the base corner ($x/R_0 = 0.0$) the agreement between experiment and computation is quite good. The experimental pressure distribution shown in Fig. 3 was numerically integrated along the boattail using a trapezoidal rule to determine an area-averaged boattail drag coefficient of 0.056. For comparison, the integrated-method-of-characteristics profile yields an average boattail drag coefficient of 0.061, which is slightly higher than the experimental result because of the rapid drop in pressure predicted at the body-boattail junction.

The measured static pressure distribution across the base of the boattailed afterbody is shown in Fig. 4 along with similar data obtained for the cylindrical afterbody.[12] In general, the two profiles are very similar, showing a slight increase in base pressure with increasing radius; however, the overall magnitudes of the pressure coefficient are substantially lower on the boattailed afterbody (reduced afterbody drag). The pressures at the outer edge of the base may be higher than at the center on account of the severe streamline curvature that undoubtedly occurs near this region. As the low-speed fluid flowing radially outward at the base becomes entrained by the high-speed shear layer near the base corner, a change in flow direction in excess of 90 deg results; for this reason, the static pressure imposed near the base corner should be increased over the pressure at the center of the base.

The base pressure distributions shown in Fig. 4 were numerically integrated using a trapezoidal rule to obtain area-averaged base drag coefficients of 0.086 and 0.102 for the boattailed and cylindrical afterbodies, respectively. When examining the benefits of afterbody boattailing relative to a cylindrical afterbody, the net afterbody drag coefficients (boattail + base) must be compared. For the present boattailed afterbody, the net afterbody drag coefficient was determined to be 0.081. For the cylindrical afterbody, the only contribution to the net afterbody form drag is from the base,

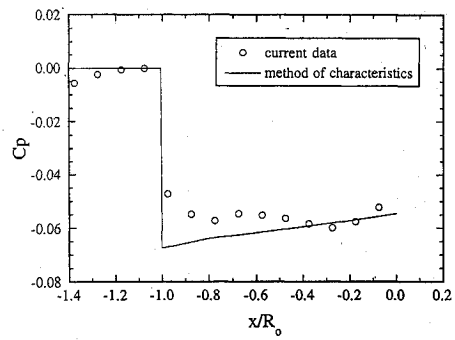

Fig. 3 Boattail pressure distribution.

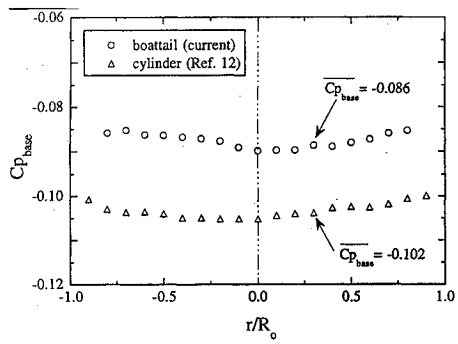

Fig. 4 Base pressure distributions for boattailed and cylindrical afterbodies.

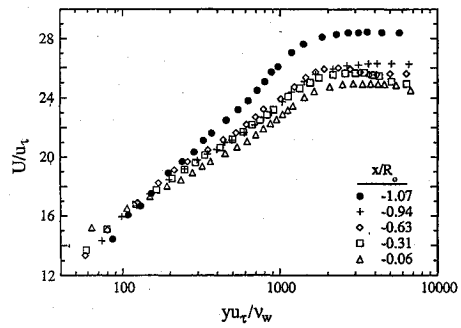

Fig. 5 Bounday-layer profiles perpendicular to boattail surface (body-boattail junction located at $x/R_0 = -1.00$).

$C_{Dnet} = C_{Dbase} = 0.102$. A comparison of the net afterbody drag coefficients for each afterbody shows a 21% reduction in drag due to afterbody boattailing. This result compares well with the data of Ref. 5, which showed a drag reduction of 25% with a similar geometry and flow conditions. From the data presented above, it is obvious that afterbody boattailing is an effective method to reduce net afterbody drag on axisymmetric bodies in supersonic flight. The fluid-dynamic effects associated with the drag reduction (increase in base pressure) have been investigated in the current study with detailed LDV measurements throughout the near-wake flowfield. These measurements are described below.

Velocity Measurements

Approach Flowfield

Mean-velocity and turbulence data have been obtained upstream of the base corner along thirteen traverses normal to the afterbody surface. These data are used to fully document the approach conditions to the near-wake flowfield as well as to determine the effects of the centered expansion at the body-boattail junction on the characteristics of the turbulent boundary layer immediately upstream of separation. The mean streamwise velocity profiles at five axial locations upstream of the base corner are plotted in conventional wall coordinates in Fig. 5 (data from only five of the thirteen traverses are shown in the figure to avoid overcrowding). By comparing the data obtained upstream of the body-boattail junction (represented by the filled symbols in the figure) with those obtained at successive axial locations along the boattail, the expansion at the body-boattail junction is shown to reduce the outer wake of the original undisturbed boundary layer and to cause a gradual reduction in the slope of the log region. Relaxation of the mean velocity downstream of the body-boattail junction appears quite rapid initially, but the general shape of the profiles appears to be slowly evolving even at the last axial station prior to separation at the base corner ($x/R_0 = -0.06$). These results are similar to those given by Ref. 9, which showed that the boundary layer downstream of a sudden expansion recovers quickly at first, with significant changes in the mean profile occurring within the first 10 boundary-layer thicknesses downstream of the expansion (this distance corresponds to the length of the boattail in the present case); a complete recovery of the mean velocity and turbulence profiles across the boundary layer generally requires a substantially longer distance.

The mean boundary layer velocity profile immediately upstream of the base corner ($x/R_0 = -0.06$) is shown in Fig. 6 with a curve fit for compressible, turbulent boundary layers given in Ref. 14. The integral boundary-layer properties as determined from the curve fit are important initial conditions to the near-wake flowfield and therefore are also included in the figure. The good agreement between the experimental data and the curve fit suggests that the boundary layer has nearly recovered (in the mean-velocity sense) from the expansion at the body-boattail junction and is approximately in equilibrium prior to separation (note that this "new" equilibrium state is different than that existing upstream of the body-boattail junction). In the present case, the boundary-layer thickness is approximately 15% of the base radius, so that axisymmetric effects on the boundary layer due to lateral surface curvature are generally quite weak. The values shown in Fig. 6 for the shape factor, wake strength parameter, and skin-friction coefficient fall within the ranges established by previ-

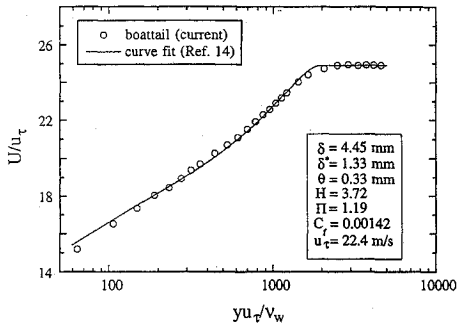

Fig. 6 Mean bounday-layer profile immediately upstream of base corner ($x/R_0 = -0.06$).

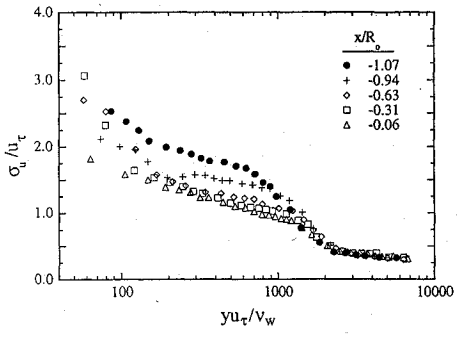

Fig. 7 Effect of expansion at body-boattail junction on streamwise rms velocity fluctuation.

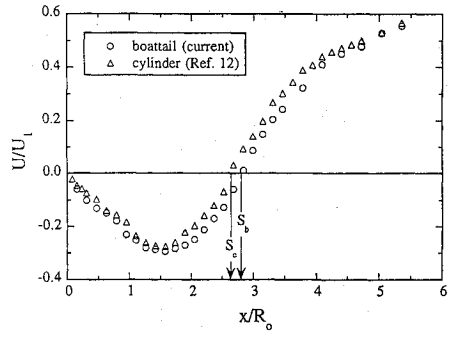

Fig. 8 Mean axial velocity along centerline: comparison between boattailed and cylindrical afterbodies.

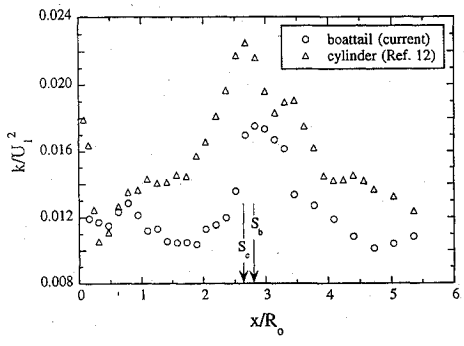

Fig. 9 Turbulent kinetic energy distributions along centerline: comparison between boattailed and cylindrical afterbodies.

ous investigators for equilibrium, compressible, turbulent boundary layers.[15] The freestream Mach number and unit Reynolds number immediately upstream of the base corner are 2.61 and 47×10^6 m^{-1}, respectively.

Although the mean velocity in the boundary layer recovers fairly quickly from the expansion at the body-boattail junction, previous experiments have shown that the turbulence properties generally recover much more slowly.[9,10] Figure 7 is a plot of the nondimensional streamwise root-mean-square (rms) velocity fluctuation (σ_u/u_τ) distribution at five axial stations along the afterbody (again, for clarity only a few traverses are shown). A significant distortion in the streamwise rms velocity fluctuation profile occurs through the sudden expansion at the body-boattail junction with an overall reduction in the magnitude of the turbulence fluctuations (as characterized by σ_u). The collapse of the data obtained at the last two axial stations upstream of the base corner seems to indicate that a "new" equilibrium state of reduced turbulence levels has been reached prior to separation. Although not shown here for conciseness, the transverse rms velocity fluctuation profiles and the primary Reynolds shear stress profiles also exhibited a significant decrease in magnitude through the expansion at the body-boattail junction.

As indicated above, the expansion at the body-boattail junction distorts both the mean velocity and turbulence quantities in the afterbody boundary layer, so that the initial conditions for the near-wake flowfield are changed considerably from those in the cylindrical afterbody case. The implications of these changes in the approach boundary-layer characteristics for the mean velocity, turbulence intensity, and Reynolds shear stress fields in the near wake of the afterbody are discussed in the following section.

Centerline Measurements

As part of the detailed documentation of the near-wake flowfield, an axial traverse on the centerline of the afterbody was completed. The LDV data were obtained in axial increments of $\Delta x/R_0 = 0.157$ from the base to the end of the test-section window (approximately $x/R_0 = 5.4$). The mean axial velocity distribution along the centerline is shown in Fig. 8 along with similar data obtained downstream of the cylindrical afterbody.[12] The rear stagnation point (reattachment location) is defined as the location where the mean axial velocity along the centerline vanishes. Note that the mean shear-layer reattachment location moves downstream when the boattail is added to the cylindrical afterbody ($S_b/R_0 = 2.81$ and $S_c/R_0 = 2.65$). This trend is consistent with the higher base pressure on the boattailed afterbody, which results in a shallower initial shear-layer angle. The mean reattachment location for both afterbodies is in general agreement with the pitot-probe measurements from Ref. 16, which found $S/R_0 = 2.9$ in a Mach 3 flow over a cylindrical afterbody. The peak reverse velocity in the separated region behind the base is approximately 29% of U_1 for the current boattailed afterbody, which is only slightly larger than that measured for the cylindrical afterbody (27% of U_1). These results are very similar to those given by Ref. 17 for a subsonic, power-off base flowfield, which supports the hypothesis of Ref. 18 that a similarity relationship may exist for the mean axial velocity along the centerline of axisymmetric bodies. In addition, the similarities in the mean axial velocity distributions at different approach Mach numbers suggest that compressibility effects are negligible in determining the mean structure of the recirculation region.

In addition to the mean axial velocity, the axial and radial rms velocity fluctuations were also determined along the centerline of each afterbody. In order to compare the overall turbulence fluctuation levels along the centerline, the turbulent kinetic energy was calculated using the following relation:

$$k = \tfrac{1}{2}\left(\sigma_u^2 + \sigma_{v_r}^2 + \sigma_{v_t}^2\right) \tag{1}$$

where $\sigma_{v_t}^2$ was set equal to $\sigma_{v_r}^2$ along the centerline. This assumption is supported by data obtained throughout the near wake, where all three components of the Reynolds normal stress were directly measured. The turbulent kinetic energy distributions along the centerline of the cylindrical[12] and boattailed afterbodies are compared in Fig. 9. Contrary to the mean axial velocity profiles shown in Fig. 8, the effect of afterbody boattailing on the centerline turbulent kinetic energy is substantial. Although both centerline distributions peak near the reattachment point as the shear layer converges on the axis, the turbulent kinetic energy is significantly reduced in the boattailed afterbody case (peak value is reduced by approximately 22%). This result suggests that the turbulence mechanisms in the near wake, and particularly in the reattaching shear layer, are attenuated by afterbody boattailing. This result stems, in part, from

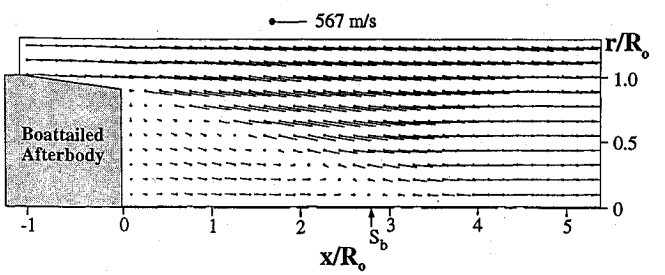

Fig. 10 Mean-velocity vector field.

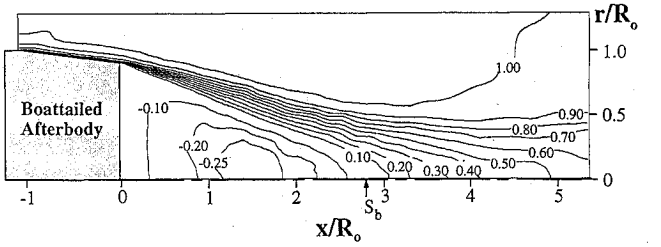

Fig. 11 Mean axial-velocity field—U/U_1.

the reduced turbulence levels in the separating boundary layer for the boattailed afterbody case. The effects of afterbody boattailing on the mean-velocity and turbulence properties throughout the near wake are discussed in more detail in the next two sections.

Near-Wake Mean-Velocity Measurements

The mean-velocity vector field throughout the near wake of the current boattailed afterbody is shown in Fig. 10. Note that in this and subsequent figures the vertical axis has been expanded by 46% compared to the horizontal axis in order to show more clearly the important features of the flowfield. To enhance the presentation of the mean-velocity field, the uniformly spaced velocity vectors shown in Fig. 10 have been generated by a linear interpolation in both x and r of the unequally spaced LDV data. The mean-velocity vector field in Fig. 10 shows qualitatively many of the features of the near-wake flowfield shown previously in Fig. 1. The freestream flow is shown to undergo a series of deflections due to the expansions at the body-boattail junction and base corner, followed by the recompression shock wave system in the near wake, which realigns the flowfield with the axis of symmetry. The general shape of the recirculation region behind the base is also clearly shown in the figure. The location of the mean reattachment point is labeled along the horizontal axis; it provides a useful marker for the relative location of many important features of the near-wake flowfield.

A contour plot of U/U_1 in the near wake is shown in Fig. 11. The growth of the shear layer downstream of the base corner is shown by the diverging contour lines, which initially are spaced very closely together, indicating large mean axial-velocity gradients in the shear layer immediately downstream of separation. It is interesting to note that the contour levels at the inner edge of the shear layer diverge rapidly from the base corner, while those at the outer edge (contour levels 0.8–1.0) diverge slowly with downstream distance. This result suggests that a two-layer description of the initial shear-layer development (suggested in Ref. 8 for attached boundary layers downstream of a rapid expansion) may be appropriate where an inner layer of high turbulence levels and large mass entrainment rates grows rapidly within an outer layer of lower turbulence levels and relatively slow development. As suggested in Fig. 11, the inner layer eventually overtakes the outer layer and consumes a majority of the overall shear layer width. The recovery of the mean-axial-velocity profile downstream of reattachment is seen to be fairly rapid; however, at the far downstream extent of the present measurements, a velocity defect of approximately 42% still exists, which indicates that full recovery of the mean axial velocity in the wake does not occur within 5 base radii. Reference 19 found that the wake in their two-dimensional base flow fully recovered (velocity defect vanished) at a downstream distance of 4.7 base heights

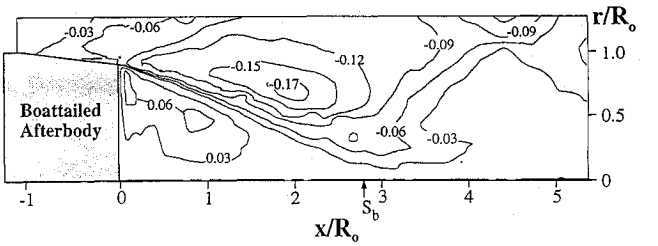

Fig. 12 Mean radial velocity field—V_r/U_1.

(equivalent to 9.4 base radii in the present case). Although full wake recovery was not achieved in the present case, the mean flow at the last axial station surveyed was found to be entirely supersonic, so that disturbances generated further downstream by the wind-tunnel geometry have no effect on the near-wake flowfield of interest.

In addition to the mean axial velocity, the mean radial velocity was also determined from the three-component LDV data; contours of V_r/U_1 are shown throughout the near wake in Fig. 12. The location of the rapid expansions at the body-boattail junction and base corner are now more clearly shown by decreasing contour levels (more negative radial velocity); the expansions appear to be well centered at these locations. Beyond the base-corner expansion fan, the mean radial velocity continues to increase in magnitude, due to axisymmetric effects, to a peak value of $0.18U_1$ at about two afterbody radii downstream. The gradual realignment of the freestream flow is shown on the right in Fig. 12 by the increasing contour levels, and the realignment appears even slower in the inner region of the shear layer, as evidenced by the persistence of a mean-radial-velocity "finger" at the lower right in the figure. This realignment pattern was also found in the cylindrical afterbody case[12] and is important in multicomponent modeling of these flowfields, as the recompression criterion provides the closure condition to the entire near-wake solution.[20] The mean-radial-velocity contours in Fig. 12 also show the acceleration of the low-speed fluid flowing radially outward (positive V_r) at the base as it becomes entrained into the shear layer near the base corner. Note the rapid change of flow direction (change in sign of the mean radial velocity) near the base corner, which, as mentioned earlier, may be responsible for the rising base pressure with increasing radius from the base center. Lastly, the increasing contour levels at the upper right in Fig. 12 mark the location of a compression wave generated by the reflection of the body-boattail junction expansion fan from a shear layer at the outer periphery of the test section. This region of the flow is entirely supersonic, so that interference with the near-wake flowfield of interest does not occur.

By comparing the mean-velocity field discussed above with that obtained downstream of a cylindrical afterbody,[12] it is found that the overall structure of the mean flowfield in these cases is qualitatively similar. However, one important difference that exists due to afterbody boattailing is a reduction in the mean shear-layer growth rate of approximately 20% from that in the cylindrical afterbody case. The growth rate of the shear layer is directly linked to the amount of mass entrainment from the recirculation region and therefore directly affects the base pressure. The reduction in shear-layer growth for the boattailed afterbody is consistent with the measured higher base pressure than for a cylindrical afterbody (16% higher in the present case) and is an important factor in determining the overall effectiveness of afterbody boattailing in reducing base drag.

Near-Wake Turbulence Measurements

In the present experiments, five of the six components of the kinematic Reynolds stress tensor have been directly measured. In this section, the primary results of these turbulence measurements will be presented. Figure 13 is a contour plot of the axial turbulence intensity throughout the near-wake flowfield. The increase in the axial turbulence intensity from the relatively low levels in the freestream marks the outer edge of the shear layer. A peak value of approximately 0.203 occurs in the subsonic portion of the shear layer, approximately 2 afterbody radii downstream of the base corner, and

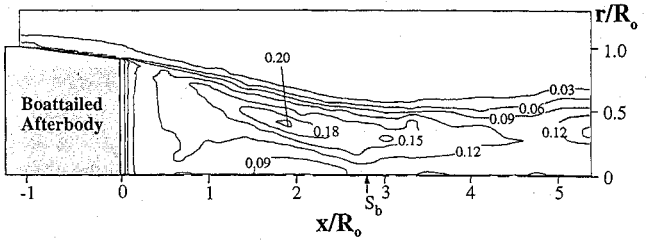

Fig. 13 Axial turbulence intensity contours—σ_u/U_1.

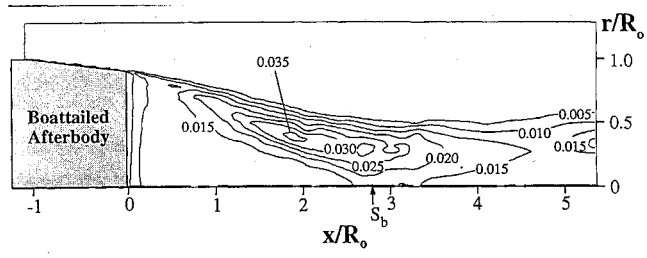

Fig. 15 Turbulent kinetic energy contours—k/U_1^2.

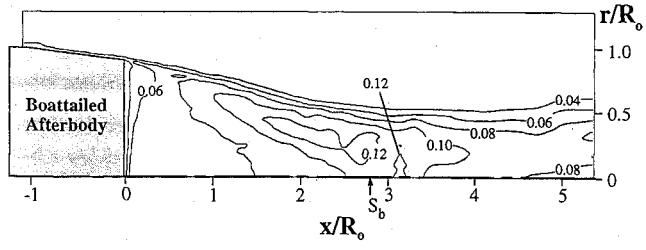

Fig. 14 Radial turbulence intensity contours—σ_{v_r}/U_1.

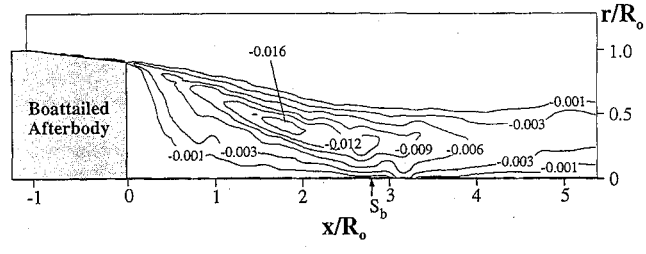

Fig. 16 Reynolds shear stress contours—$\langle u'v'_r \rangle / U_1^2$.

represents a reduction from the peak level in the cylindrical afterbody case[12] of nearly 8%. In fact, throughout the shear-layer and wake regions of the boattailed afterbody near wake, the axial turbulence intensity is reduced from the cylindrical afterbody case. This is most likely a result of the reduced turbulence levels in the boundary layer upstream of the base corner. In addition, the reduced strength of the base-corner expansion fan in the boattailed afterbody case results in less distortion of the mean-velocity profiles and reduced turbulence production in the initial portions of the shear layer.[21] The axial turbulence intensity decays through the reattachment region in the present case, which is in contrast to data obtained for a compressible shear layer reattaching onto a solid wall, where it has been shown[22,23] that the axial turbulence intensity peaks downstream of the reattachment point. These differences in the locations for the peak axial turbulence intensity may be attributed to the difference in the boundary condition between the two cases. In the solid-wall case, the velocity constraint at the wall ($v = 0$) holds in an instantaneous sense, so that the mean velocity and rms velocity fluctuations both must vanish at the wall. However, in the compliant-surface reattachment of the present case, the velocity constraint at the fictitious surface requires that the mean transverse velocity vanish but not the instantaneous transverse velocity, so that a nonzero transverse rms velocity fluctuation exists. The axial turbulence intensity also peaked upstream of the reattachment point for the cylindrical afterbody case.[12] Interestingly, peak turbulence intensities have also been shown to occur upstream of reattachment for subsonic shear layers reattaching onto a solid wall.[24]

In addition to the axial turbulence intensity, the radial and tangential turbulence intensities were also determined from the LDV data; the radial turbulence intensity contours are shown in Fig. 14. The qualitative trends are similar to those of the axial turbulence intensity, with relatively large values in the shear layer that decay through the reattachment region into the downstream wake. A peak radial value of 0.129 occurs slightly upstream of reattachment and represents a 17% decrease from the peak value measured in the cylindrical afterbody case.[12] Note that the overall magnitudes of the radial turbulence intensity are smaller than those of the axial component, with a typical anisotropy, σ_u/σ_{v_r}, of 1.6–2.0 in the shear layer. Throughout the recirculation region, the radial turbulence intensity remains fairly uniform at levels reduced from those in the shear layer. The tangential turbulence intensity distribution is similar to that shown in Fig. 14 for the radial turbulence intensity, with a peak value of 0.133 occurring near the reattachment point. The addition of the boattail caused little change in the peak tangential turbulence intensity (1.4% reduction), even though the other two turbulence intensity components were significantly reduced. Throughout the shear layer, a radial-to-tangential anisotropy ratio ($\sigma_{v_r}/\sigma_{v_t}$) of approximately unity is maintained; thus, the magnitude ordering of the Reynolds normal stresses in the present case is $\sigma_u > \sigma_{v_r} \sim \sigma_{v_t}$, which indicates the preferential orientation of the turbulence field in the axial direction.

Utilizing the three turbulence intensity distributions measured in the present study, the turbulent kinetic energy [see Eq. (1)] has been determined and is shown in Fig. 15. As mentioned above, the axial turbulence intensity dominates the turbulence field, so the turbulent kinetic energy contours shown in Fig. 15 appear similar to those of the axial turbulence intensity shown in Fig. 13. The peak value of $k/U_1^2 = 0.0359$ occurs upstream of reattachment in the subsonic region of the shear layer. This global maximum in turbulent kinetic energy is significantly smaller than the value given in Ref. 19, where a peak turbulent kinetic energy of 0.07 was found near reattachment in the two-dimensional base flow study. The significant difference between these two values is most likely a result of the much weaker base-corner expansion fan in the present case, which results in less turbulence production immediately downstream of separation. In fact, Ref. 25 reports a measured peak turbulent kinetic energy of approximately 0.042 in the reattachment region of a supersonic shear layer that had been separated at constant pressure from a backstep (i.e., no expansion at the separation point). The peak value in the present case also represents an 18% reduction from the peak turbulent kinetic energy measured in the cylindrical afterbody case.[12] The measured reduction in turbulence levels in the shear layer results in less mass entrainment from the recirculation region for the boattailed afterbody case, which, as mentioned previously, is consistent with the reduction in measured shear-layer growth rate (approximately 20%) and increased base pressure. In the recirculation region behind the base, the turbulent kinetic energy is fairly uniform at values significantly smaller than those in the shear layer.

In addition to the turbulence intensity components presented above, the axial-radial and axial-tangential Reynolds shear stresses have been measured directly. The measured axial-radial shear stress was larger than the measured axial-tangential shear stress by approximately an order of magnitude in the high-turbulence regions of the shear layer. Contours of the dimensionless axial-radial shear stress are shown in Fig. 16. As in the axial turbulence intensity contours shown previously, the peak dimensionless shear stress magnitude occurs upstream of reattachment and takes a value of 0.0175, which represents an 8% decrease from the peak value measured in the cylindrical afterbody case.[12] In addition, the peak shear stress measured in the current study is significantly smaller than that measured in Ref. 19 in the two-dimensional base flow study. Throughout the recirculation region, the shear stress magnitudes are small, indicating the absence of any significant large-scale turbulence in the separation bubble downstream of the base. The locus of peak shear

Table 1 Comparison of peak values of turbulence quantities

Quantity	Cylindrical afterbody	Boattailed afterbody	Difference, %
σ_u/U_1	0.220	0.203	−7.7
σ_{v_r}/U_1	0.156	0.129	−17.3
σ_{v_t}/U_1	0.135	0.133	−1.4
k/U_1^2	0.0440	0.0359	−18.4
$-\langle u'v_r'\rangle/U_1^2$	0.0190	0.0175	−7.9

stress magnitudes at each axial station in the near wake consistently lies in the subsonic region of the shear layer, which indicates the importance of large-scale turbulent structures in the entrainment of fluid from the recirculation region.

In general, the effect of afterbody boattailing is to reduce the overall turbulence levels throughout the near-wake flowfield relative to a cylindrical afterbody. Table 1 presents a summary of the peak values of the primary turbulence quantities obtained for the current boattailed afterbody and those obtained previously for the cylindrical afterbody.[12] The addition of the boattail is shown to significantly reduce both the axial and radial turbulence intensities, with the strongest effect occurring in the radial component. In addition, the turbulent kinetic energy and Reynolds shear stress are reduced by afterbody boattailing. From an analysis of the turbulence production in the near wake of both the cylindrical and boattailed afterbodies,[21] the decrease in near-wake turbulence for the boattailed afterbody is found to be due, in part, to the reduced strength of the base-corner expansion fan, which directly affects the mean-velocity gradient (and therefore turbulence production) in the initial portion of the shear layer. Of course, the reduced turbulence in the boattailed afterbody boundary layer also plays a role in the overall reduction in turbulence in the near wake of the boattailed afterbody. The practical significance of the reduced turbulence in the present case is the substantial reduction in mass entrainment from the recirculation region (shear-layer growth rate reduced by approximately 20%), which directly implies a higher base pressure.

Conclusions

An experimental investigation of the near-wake flowfield behind a conical boattailed afterbody in supersonic flow has been presented. The primary objectives of this study are to investigate the fluid-dynamic effects of afterbody boattailing and how they relate to the increase in base pressure on conventional unpowered missiles and projectiles in supersonic flight. The experimental procedure followed during the investigation was to obtain detailed nonintrusive experimental data on a simplified configuration (i.e., without afterbody control fins) both with and without a boattail. The data include flow visualization photographs, measurements of the mean static pressure on the afterbody and base, and three-component LDV measurements throughout the near wake. A second objective of this study was to provide experimental data of sufficient detail and quality that could be used in numerical validation studies. Toward this end, the entire set of data presented in this paper has been tabulated in an easily readable format and is available on disk from the authors. From the data presented herein, the following conclusions can be drawn:

1) Afterbody boattailing is an effective means of decreasing the net afterbody drag on unpowered missiles and projectiles in supersonic flight. In the present case, the addition of a conical boattail resulted in a net afterbody drag reduction of 21% from a cylindrical afterbody at the same approach Mach number and Reynolds number.

2) The rapid expansion at the body-boattail junction in supersonic flow can significantly alter the mean velocity and turbulence distributions in the afterbody boundary layer. In addition to a reduction of the outer wake component of the mean boundary-layer velocity profile, the rapid expansion causes a decrease in the turbulence intensity and Reynolds shear stress throughout the boundary layer, which, if the boattail length is sufficiently short, can result in substantial changes in the boundary-layer conditions at separation.

3) The mean velocity in the near wake of unpowered axisymmetric bodies is qualitatively unaffected by afterbody boattailing. The most significant quantitative effect of boattailing is a reduction in the mean shear-layer growth rate (approximately 20% in the present case), which is a result of reduced mass entrainment rates from the recirculation region behind the base. Obviously, this mechanism has direct influence on the base pressure and therefore is an important effect of afterbody boattailing in supersonic flow.

4) Turbulence levels in the separated shear layer are significantly reduced (e.g., 18% reduction in the turbulent kinetic energy) by afterbody boattailing due to the diminished fluctuations in the boundary layer at separation and to the reduced strength of the expansion fan at the base corner, which reduces turbulence production in the initial portion of the shear layer. In general, the axial Reynolds normal stress dominates the near-wake turbulence field, with the radial and tangential normal stresses being approximately equal. Strong peaks in the axial Reynolds normal stress and Reynolds shear stress occur in the subsonic region of the shear layer at an axial location upstream of the reattachment point.

Acknowledgments

This work was supported by the U.S. Army Research Office (Contract No. DAAL03-90-G-0021) with Thomas L. Doligalski serving as contract monitor.

References

[1]Rollstin, L., "Measurement of Inflight Base Pressure on an Artillery-Fired Projectile," AIAA Paper 87-2427, Aug. 1987.

[2]Phillips, W. P., Compton, H. R., and Findlay, J. T., "Base Drag Determination for STS Flights 1–5," AIAA Paper 83-2719, Nov. 1983.

[3]Addy, A. L., and White, R. A., "Optimization of Drag Minimums Including Effects of Flow Separation," *ASME Transactions: Journal of Engineering for Industry*, Vol. 95, No. 1, 1973, pp. 360–364.

[4]Reid, J., and Hastings, R. C., "Experiments on the Axi-Symmetric Flow over Afterbodies and Bases at $M = 2.0$," Royal Aircraft Establishment, RAE Rept. Aero. 2628, Farnborough, England, UK, 1959.

[5]Rubin, D. V., Brazzel, C. E., and Henderson, J. H., "The Effects of Jet Plume and Boattail Geometry on Base and Afterbody Pressures of a Body of Revolution at Mach Numbers of 2.0 to 3.5," U.S. Army Missile Command, RD-TR-70-5, Redstone Arsenal, AL, April 1970.

[6]Agrell, J., and White, R. A., "An Experimental Investigation of Supersonic Axisymmetric Flow over Boattails Containing a Centered Propulsive Jet," The Aeronautical Research Institute of Sweden (FFA), TN AU-913, Dec. 1974.

[7]Viswanath, P. R., and Narasimha, R., "Two-Dimensional Boat-Tailed Bases in Supersonic Flow," *The Aeronautical Quarterly*, Vol. 25, No. 3, 1974, pp. 210–224.

[8]Hampton, L. P., and White, R. A., "The Effect of Sudden Expansions and Compressions on Turbulent Boundary Layer Momentum Thickness in Supersonic Flow," American Society of Mechanical Engineers, Paper 86-WA/FE-11, Dec. 1986.

[9]Dussauge, J. P., and Gaviglio, J., "The Rapid Expansion of a Supersonic Turbulent Flow: Role of Bulk Dilatation," *Journal of Fluid Mechanics*, Vol. 174, Jan. 1987, pp. 81–112.

[10]Smith, D. R., and Smits, A. J., "The Rapid Expansion of a Turbulent Boundary Layer in a Supersonic Flow," *Journal of Theoretical and Computational Fluid Dynamics*, Vol. 2, Nos. 5/6, 1991, pp. 319–328.

[11]Arnette, S. A., Samimy, M., and Elliott, G. S., "The Effect of Expansion on the Large Scale Structure of a Compressible Turbulent Boundary Layer," AIAA Paper 93-2991, July 1993.

[12]Herrin, J. L., and Dutton, J. C., "Supersonic Base Flow Experiments in the Near Wake of a Cylindrical Afterbody," *AIAA Journal*, Vol. 32, No. 1, 1994, pp. 77–83.

[13]Maise, G., "Wave Drag of Optimum and Other Boattails," *Journal of Aircraft*, Vol. 7, No. 5, 1970, pp. 477–478.

[14]Sun, C. C., and Childs, M. E., "A Modified Wall Wake Velocity Profile for Turbulent Compressible Boundary Layers," *Journal of Aircraft*, Vol. 10, No. 6, 1973, pp. 381–383.

[15]Fernholz, H. H., and Finley, P. J., "A Critical Commentary on Mean Flow Data for Two-Dimensional Compressible Turbulent Boundary Layers," AGARDograph No. 253, AGARD, May 1980.

[16]Neale, D. H., Hubbartt, J. E., Strahle, W. C., and Wilson, W. W., "Effects of External Compression on an Axisymmetric Turbulent Near Wake," *AIAA Journal*, Vol. 16, No. 9, 1978, pp. 940–947.

[17]Delery, J., "ONERA Research on Afterbody Viscid/Inviscid Interaction with Special Emphasis on Base Flows," *Proceedings of the Symposium on Rocket/Plume Fluid Dynamic Interactions, Vol. III—Flow Fields*, Univ. of Texas at Austin, Austin, TX, 1983; also Fluid Dynamics Labs. Rept. 83-104, April 1983.

[18]Merz, R. A., Page, R. H., and Przirembel, C. E. G., "Subsonic Axisymmetric Near-Wake Studies," *AIAA Journal*, Vol. 16, No. 7, 1978, pp. 656–662.

[19]Amatucci, V. A., Dutton, J. C., Kuntz, D. W., and Addy, A. L., "Two-Stream, Supersonic, Wake Flowfield behind a Thick Base, Part I: General Features," *AIAA Journal*, Vol. 30, No. 8, 1992, pp. 2039–2046.

[20]Korst, H. H., "Axisymmetric Wakes in Supersonic Unpowered Missile Flight," *Proceedings of the Symposium on Rocket/Plume Fluid Dynamic Interactions, Vol. III—Flow Fields*, Univ. of Texas at Austin, Austin, TX, 1983; also Fluid Dynamics Labs. Rept. 83-104, April 1983.

[21]Herrin, J. L., "An Experimental Investigation of Supersonic Axisymmetric Base Flows Including the Effects of Afterbody Boattailing," Ph.D. Thesis, Univ. of Illinois at Urbana–Champaign, July 1993.

[22]Hayakawa, K., Smits, A. J., and Bogdonoff, S. M., "Turbulence Measurements in a Compressible Reattaching Shear Layer," *AIAA Journal*, Vol. 22, No. 7, 1984, pp. 889–895.

[23]Abu-Hijleh, B., and Samimy, M., "An Experimental Study of a Reattaching Supersonic Shear Layer," AIAA Paper 89-1801, June 1989.

[24]Eaton, J. K., and Johnston, J. P., "A Review of Research on Subsonic Turbulent Flow Reattachment," *AIAA Journal*, Vol. 19, No. 9, 1981, pp. 1093–1100.

[25]Samimy, M., Petrie, H. L., and Addy, A. L., "A Study of Compressible Turbulent Reattaching Free Shear Layers," *AIAA Journal*, Vol. 24, No. 2, 1986, pp. 261–267.